Probing the neutrino seesaw scale with gravitational waves

Bartosz Fornal, Dyori Polynice, and Luka Thompson
Department of Chemistry and Physics, Barry University, Miami Shores, Florida 33161, USA

(Received 27 June 2024; accepted 4 October 2024; published 13 November 2024)

Neutrinos are the most elusive particles of the Standard Model. The physics behind their masses remains unknown and requires introducing new particles and interactions. An elegant solution to this problem is provided by the seesaw mechanism. Typically considered at a high scale, it is potentially testable in gravitational wave experiments by searching for a spectrum from cosmic strings, which offers a rather generic signature across many high-scale seesaw models. Here we consider the possibility of a low-scale seesaw mechanism at the PeV scale, generating neutrino masses within the framework of a model with gauged U(1) lepton number. In this case, the gravitational wave signal at high frequencies arises from a first order phase transition in the early Universe, whereas at low frequencies it is generated by domain wall annihilation, leading to a double-peaked structure in the gravitational wave spectrum. The signals discussed here can be searched for in upcoming experiments, including gravitational wave interferometers, pulsar timing arrays, and astrometry observations.

DOI: 10.1103/PhysRevD.110.095013

I. INTRODUCTION

The Standard Model [1–8] is a triumph of theoretical and experimental elementary particle physics in describing the world at the subatomic level. It also enables us to dive back in time and understand what happened in the Universe starting from roughly one trillionth of a second after the big bang. Despite those undeniable successes, a few key observations still escape theoretical understanding, with the most pressing ones, on the particle physics end, considering questions about the nature of dark matter, the origin of the matter-antimatter asymmetry, and the mechanism behind neutrino masses. While dark matter [9–11] may be entirely decoupled from the Standard Model and direct detection experiments may never see it, the other two problems require additional ingredients and interactions with the Standard Model particle content, confirming that the currently established elementary particle picture is not yet complete. In this work we focus on the neutrino mass puzzle.

Several frameworks for generating small neutrino masses have been proposed. The simplest one is the type I seesaw mechanism [12–15], which requires introducing only right-handed neutrinos with a large mass term,

$$-\mathcal{L}_I \supset y_\nu \bar{l}_L \tilde{H} \nu_R + M \overline{\nu_R^c} \nu_R + \text{H.c.}, \tag{1}$$

leading to the left-handed neutrino masses $m_\nu \sim (y_\nu v)^2/M$, where v is the Higgs vacuum expectation value (VEV). The other tree-level mechanisms include type II seesaw [16–19] involving a new $SU(2)_L$ triplet scalar Δ,

$$-\mathcal{L}_{II} \supset y_\nu \overline{l_L^c} i\tau_2 \Delta l_L + \mu H^T i\tau_2 \Delta^\dagger H + \text{H.c.}, \tag{2}$$

resulting in neutrino masses $m_\nu \sim y_\nu \mu v_0^2/M_\Delta^2$, where v_0 is the VEV of the neutral component of Δ, and type III seesaw [20] with new heavy $SU(2)_L$ triplet fermions ρ,

$$-\mathcal{L}_{III} \supset y_\nu l_L i\tau_2 \rho_L H + \text{Tr}(\rho M_\rho \rho) + \text{H.c.}, \tag{3}$$

yielding neutrino masses $m_\nu \sim (y_\nu v)^2/M_\rho$. The commonly considered neutrino mass generation mechanism at the loop level is the Zee model [21] requiring a new electroweak singlet and an electroweak doublet scalar.

Given that the Standard Model is a gauge theory with baryon and lepton number as accidental global symmetries, it is natural to consider a framework in which one of them or both are promoted to be gauge symmetries. The efforts to do this started 50 years ago [22], with only a few other attempts [23–26] until fairly recently, when modern phenomenologically consistent models of this type were constructed [27–29]. This idea was further expanded to supersymmetric theories [30], unified models [31,32], and generalized to non-Abelian gauged lepton number [33]. Detailed analyses of dark matter candidates in models with gauged baryon/lepton number were conducted in [34–36], and solutions to the matter-antimatter asymmetry puzzle were considered through a new sphaleron process [33] and high-scale leptogenesis [37].

The nontrivial symmetry breaking pattern in theories with gauged baryon and lepton number presents an opportunity to search for signatures of those models in gravitational wave experiments. Indeed, the 2016 first direct detection of gravitational waves by the Laser Interferometer Gravitational Wave Observatory (LIGO) and Virgo Collaboration [38] brought new hope for particle physics by searching for a stochastic gravitational wave background from the early Universe arising from first order phase transitions [39], dynamics of cosmic strings [40,41], domain wall annihilation [42], and inflation [43]. Among those, the processes resulting in signatures that most heavily depend on the particle physics details are first order phase transitions and domain wall annihilation.

First order phase transitions occur when a new true vacuum is formed with an energy density lower than that of the high-temperature false vacuum, and both are separated by a potential barrier. When the Universe undergoes a transition from the false to the true vacuum, this triggers the nucleation of bubbles, which expand and fill up the Universe. During this process, gravitational waves are generated from sound waves, bubble wall collisions, and turbulence. This has been studied in the context of numerous particle physics models [44–88] (for a review, see [89–91], and for constraints from LIGO/Virgo data, see [92]). Among those works, the first order phase transition gravitational wave signatures of various models with separately gauged baryon and lepton number symmetries were studied in [70,83,86,87].

If there existed more than one vacuum the Universe could transition to, topological defects such as domain walls would be produced. Those are two-dimensional field configurations formed at the boundaries of regions of different vacua. To avoid overclosing the Universe, domain walls need to undergo annihilation, which is possible if there exists a slight energy density mismatch (potential bias) between the vacua. The resulting stochastic gravitational wave background depends both on the scale of the symmetry breaking and the potential bias determined by the details of the scalar potential of the model. Such signatures have been considered in many particle physics models [86,87,93–104] (for a review, see [105], and for the bounds from LIGO/Virgo data, see [106]).

Since the theories for neutrino masses usually studied in the literature are high-scale seesaw models [allowing for an $\mathcal{O}(1)$ neutrino Yukawa coupling], the commonly considered gravitational wave signatures are those arising from cosmic strings, which are topological structures forming when a U(1) symmetry is broken and correspond to one-dimensional field configurations along the direction of the unbroken symmetry. The reason is that gravitational radiation from the dynamics of cosmic strings provides signals from models with high symmetry breaking scales which are within the reach of current and upcoming gravitational wave experiments [70,107–117] (for a review, see [118], and for the limits from LIGO/Virgo data, see [119]). Nevertheless, cosmic string signatures are generic and depend only on the symmetry breaking scale; thus, they are not useful in probing particle physics details.

In this paper, we consider the seesaw mechanism at the PeV scale within the framework of the model with gauged lepton number proposed in [120]. The theory predicts a first order phase transition in the early Universe and subsequent formation of domain walls which undergo annihilation. This results in a very unique scenario when a double-peaked gravitational wave signature is expected from just a single U(1) symmetry breaking. The peak in the spectrum arising from the first order phase transition appears at high frequencies and is testable in future experiments such as Cosmic Explorer (CE) [121], Einstein Telescope (ET) [122], DECIGO [123], and Big Bang Observer (BBO) [124]. Additionally, the peak from domain wall annihilation is within the reach of the Laser Interferometer Space Antenna (LISA) [125] and the other upcoming space-based interferometer μARES [126], pulsar timing arrays NANOGrav [127] and SKA [128], and the astrometry experiments Theia [129] and Gaia [130,131].

We begin by describing the model in Sec. II, including the particle content of the theory, symmetry breaking pattern, the resulting seesaw mechanism, and the dark matter particle. In Sec. III, we determine the shape of the effective potential and provide formulas for deriving the parameters of the first order phase transition, followed by a discussion of the resulting gravitational wave spectrum in Sec. IV. The following Secs. V and VI are devoted to describing the formation of domain walls and the gravitational wave signal from their subsequent annihilation. The final gravitational wave signal of the model is discussed in Sec. VII, followed by a brief summary in Sec. VIII.

II. THE MODEL

A natural gauge extension of the Standard Model which can accommodate the type I seesaw mechanism for the neutrinos is based on the symmetry [120]

$$\mathrm{SU}(3)_c \times \mathrm{SU}(2)_L \times \mathrm{U}(1)_Y \times \mathrm{U}(1)_\ell, \tag{4}$$

where $\mathrm{U}(1)_\ell$ is gauged lepton number.

A. Extra fermionic representations

To cancel the gauge anomalies, the following new fermions are added to the Standard Model:

$$\begin{aligned}
&\Psi_L = \left(1,2,-\frac{1}{2},\ell_1\right), \quad \Psi_R = \left(1,2,-\frac{1}{2},\ell_2\right),\\
&\eta_L = (1,1,-1,\ell_2), \quad \eta_R = (1,1,-1,\ell_1),\\
&\chi_L = (1,1,0,\ell_2), \quad \chi_R = (1,1,0,\ell_1), \quad \nu_{Ri} = (1,1,0,1),
\end{aligned} \tag{5}$$

where $\ell_1 - \ell_2 = -3$. We also assume, following [120], that $\ell_1 \neq -\ell_2$ and $\ell_1, \ell_2 \neq \pm 1$. The corresponding Lagrangian fermionic kinetic terms are

$$\mathcal{L}^f_{\rm kin} = i\overline{\Psi}_L \not{D} \Psi_L + i\bar{\Psi}_R \not{D} \Psi_R + i\bar{\eta}_L \not{D} \eta_L + i\bar{\eta}_R \not{D} \eta_R + i\bar{l}_L \not{D} l_L + i\bar{e}_R \not{D} e_R + i\bar{\nu}_R \not{D} \nu_R, \quad (6)$$

where the covariant derivative $D_\mu = \partial_\mu + i g_\ell L_\mu L$, and after symmetry breaking L_μ gives rise to the new gauge boson Z_ℓ.

B. Symmetry breaking and type I seesaw

The gauged lepton number symmetry $\mathrm{U}(1)_\ell$ is broken when the two complex scalar fields,

$$S = (1, 1, 0, 3), \qquad \phi = (1, 1, 0, -2) \quad (7)$$

develop VEVs $\langle S \rangle = v_S/\sqrt{2}$ and $\langle \phi \rangle = v_\phi/\sqrt{2}$, respectively. This provides masses to the new fermions through the terms

$$-\mathcal{L}^f_Y = y_\Psi \bar{\Psi}_R S \Psi_L + y_\eta \bar{\eta}_L S \eta_R + y_\chi \bar{\chi}_L S \chi_R + y_1 \bar{\Psi}_R H \eta_L + y_2 \bar{\Psi}_L H \eta_R + y_3 \bar{\Psi}_R \tilde{H} \chi_L + y_4 \bar{\Psi}_L \tilde{H} \chi_R + y_\nu \bar{l}_L \tilde{H} \nu_R + Y_\nu \overline{\nu^c_R} \phi \nu_R + \mathrm{H.c.}, \quad (8)$$

where the last line introduces the type I seesaw mechanism, with the resulting neutrino mass matrix

$$\mathcal{M}_\nu = \frac{v^2}{2\sqrt{2} v_\phi} y_\nu Y_\nu^{-1} y_\nu^T. \quad (9)$$

In our analysis, we consider the $\mathrm{U}(1)_\ell$ breaking scale

$$v_\ell \equiv \sqrt{v_S^2 + v_\phi^2} \sim 1 \text{ PeV}. \quad (10)$$

Assuming that the elements of the Y_ν matrix are $\mathcal{O}(1)$, the neutrino Yukawa matrix entries required to reproduce the measured neutrino mass splittings are

$$y_\nu \sim 10^{-5}, \quad (11)$$

which is larger than the Standard Model electron Yukawa.

C. Scalar potential and boson masses

The scalar potential for the singlet scalars can be written as

$$V(S, \phi) = -\mu_S^2 |S|^2 + \lambda_S |S|^4 - \mu_\phi^2 |\phi|^2 + \lambda_\phi |\phi|^4 + \lambda_{S\phi} |S|^2 |\phi|^2 + \left(\frac{\lambda_M}{\Lambda} S^2 \phi^3 + \mathrm{H.c.} \right), \quad (12)$$

where we included a dimension-five term, as in [120], permitted by the quantum numbers of S and ϕ, small compared to the other terms $\lambda_M/\Lambda \ll 1/v_S, 1/v_\phi$. We also assumed that the terms coupling the heavy scalars to the Higgs are small.

Upon symmetry breaking, the mass of Z_ℓ is given by

$$m_{Z_\ell} = g_\ell \sqrt{9 v_S^2 + 4 v_\phi^2}. \quad (13)$$

The squared masses for the two CP-even scalars are

$$m^2_{\rm even} = \lambda_S v_S^2 + \lambda_\phi v_\phi^2 \pm \sqrt{(\lambda_S v_S^2 - \lambda_\phi v_\phi^2)^2 + (\lambda_{S\phi} v_S v_\phi)^2}. \quad (14)$$

There are also two CP-odd scalars—one is the Goldstone boson that becomes the longitudinal component of Z_ℓ, and the other is the Majoron with mass

$$m_J = \sqrt{\frac{\lambda_M v_\phi}{2\sqrt{2}\Lambda} (9 v_S^2 + 4 v_\phi^2)}. \quad (15)$$

Constraints on the Majoron mass and couplings to neutrinos were studied in [132], and for our choice of symmetry breaking scale, they are all satisfied.

D. Dark matter

After the $\mathrm{U}(1)_\ell$ gauge symmetry is spontaneously broken, the model exhibits an accidental global U(1) symmetry under which the new fields transform according to

$$\Psi_L \to e^{i\theta} \Psi_L, \quad \Psi_R \to e^{i\theta} \Psi_R, \quad \eta_L \to e^{i\theta} \eta_L, \quad \eta_R \to e^{i\theta} \eta_R, \quad \chi_L \to e^{i\theta} \chi_L, \quad \chi_R \to e^{i\theta} \chi_R. \quad (16)$$

Because of this residual symmetry, the lightest field among the new fermions remains stable. If it is also a Standard Model singlet, such as χ, it becomes a good dark matter candidate. We assume that the dark matter mass is below the nucleation temperature scale, so that it remains in equilibrium during the phase transition, and the standard weakly interacting massive particle freeze-out scenario is realized.

As argued in [120], to remain consistent with the observed dark matter relic abundance of $h^2 \Omega_{\rm DM} \approx 0.12$ [133], for most of the dark matter annihilation channels an upper bound on the $\mathrm{U}(1)_\ell$ breaking scale arises. For instance, assuming the s-channel annihilation,

$$\bar{\chi} \chi \to Z^*_\ell \to \bar{l} l, \quad (17)$$

perturbativity of couplings requires that $m_{Z_\ell} \lesssim 30$ TeV. Nevertheless, there are other annihilation channels that are not velocity suppressed, e.g., the t-channel annihilation via

$$\bar{\chi}\chi \to H_i H_j. \tag{18}$$

The Yukawa couplings y_3 and y_4 in Eq. (8) do not need to be small, and can lead to a sufficiently large dark matter annihilation cross section through the channel in Eq. (18) even when the symmetry is broken at the high scale ∼PeV (see, e.g., the discussion in [35]).

III. FIRST ORDER PHASE TRANSITION

To determine the range of parameters for which a first order phase transition occurs in the model, one first needs to find the shape of the effective potential, including its dependence on the temperature. In our case, there are two scalar fields participating in the breaking of $U(1)_\ell$. Denoting by $\vec{\varphi} = (\varphi_S, \varphi_\phi)^T$ the background fields corresponding to S and ϕ, respectively, the effective potential takes the form,

$$\begin{aligned} V_{\rm eff}(\vec{\varphi}, T) = &-\frac{1}{2}\left(\lambda_S v_S^2 + \frac{1}{2}\lambda_{S\phi} v_\phi^2\right)\varphi_S^2 + \frac{1}{4}\lambda_S \varphi_S^4 - \frac{1}{2}\left(\lambda_\phi v_\phi^2 + \frac{1}{2}\lambda_{S\phi} v_S^2\right)\varphi_\phi^2 + \frac{1}{4}\lambda_\phi \varphi_\phi^4 + \frac{1}{4}\lambda_{S\phi}\varphi_S^2\varphi_\phi^2 \\ &+ \sum_i \frac{n_i}{64\pi^2} m_i^4(\varphi_S, \varphi_\phi)\left[\log\left(\frac{m_i^2(\varphi_S, \varphi_\phi)}{\Lambda_\ell^2}\right) - c_i\right] + \frac{T^4}{2\pi^2}\sum_i n_i \int_0^\infty dx\, x^2 \log\left(1 \mp e^{-\sqrt{x^2 + m_i^2(\varphi_S,\varphi_\phi)/T^2}}\right) \\ &+ \frac{T}{12\pi}\sum_j n_j' \{m_j^3(\varphi_S, \varphi_\phi) - [m^2(\varphi_S, \varphi_\phi) + \Pi(T)]_j^{\frac{3}{2}}\} + \delta m_S^2 \varphi_S^2 + \delta m_\phi^2 \varphi_\phi^2 + \delta\lambda_S \varphi_S^4 + \delta\lambda_\phi \varphi_\phi^4 + \delta\lambda_{S\phi}\varphi_S^2\varphi_\phi^2. \end{aligned} \tag{19}$$

The first line of Eq. (19) correspond to the tree-level part of the potential determined using the minimization conditions. The first term in the second line reflects the one-loop Coleman-Weinberg zero-temperature contribution $V_{\rm CW}$ in the $\overline{\rm MS}$ renormalization scheme [134]; the sum is over all particles charged under $U(1)_\ell$, with $m_i(\varphi_S, \varphi_\phi)$ being their field-dependent masses, n_i denoting the corresponding number of degrees of freedom (with a negative sign for fermions), $c_i = 3/2$ for scalar and fermions, $c_i = 5/6$ for gauge bosons, and Λ_ℓ being the renormalization scale which we take to be at the $U(1)_\ell$ breaking scale. The next two sums correspond to the finite temperature contribution, with the plus sign corresponding to bosons and the minus sign to fermions, the sum over i including all particles charged under $U(1)_\ell$ and the sum over j involving only bosons, n_j' denoting all degrees of freedom for scalars and only longitudinal ones for vector bosons, $\Pi(T)$ being the thermal mass matrix, and the subscript j for $[m^2(\varphi_S, \varphi_\phi) + \Pi(T)]$ in the last line denoting the eigenvalues. Finally, the last line includes also the counterterm contributions $V_{\rm CT}$, which we determine from the conditions

$$\begin{aligned} &\frac{\partial V_{\rm CT}}{\partial\varphi_S} + \frac{\partial V_{\rm CW}}{\partial\varphi_S} = 0, \qquad \frac{\partial V_{\rm CT}}{\partial\varphi_\phi} + \frac{\partial V_{\rm CW}}{\partial\varphi_\phi} = 0, \\ &\frac{\partial^2 V_{\rm CT}}{\partial\varphi_S^2} + \frac{\partial^2 V_{\rm CW}}{\partial\varphi_S^2} = 0, \qquad \frac{\partial^2 V_{\rm CT}}{\partial\varphi_\phi^2} + \frac{\partial^2 V_{\rm CW}}{\partial\varphi_\phi^2} = 0, \\ &\frac{\partial^2 V_{\rm CT}}{\partial\varphi_S\partial\varphi_\phi} + \frac{\partial^2 V_{\rm CW}}{\partial\varphi_S\partial\varphi_\phi} = 0, \end{aligned} \tag{20}$$

and, to consistently include the contribution of the Goldstone bosons, we follow the procedure outlined in [135].

Because of choosing a high symmetry breaking scale, we can assume that the Yukawa couplings y_Ψ, y_η, and y_χ are small, consistent with the experimental constraints on the new fermions, so that their contribution does not affect the shape of the effective potential considerably. The field-dependent squared mass for the gauge boson Z_ℓ is

$$m_{Z_\ell}^2(\varphi_S, \varphi_\phi) = g_\ell^2(9\varphi_S^2 + 4\varphi_\phi^2), \tag{21}$$

and the corresponding numbers of degrees of freedom are $n_{Z_\ell} = 3$ and $n'_{Z_\ell} = 1$. In the case of the CP-even scalars, their field-dependent squared mass matrix is given by

$$m_{\rm even}^2(\varphi_S, \varphi_\phi) = \begin{pmatrix} 2\lambda_S\varphi_S^2 & \lambda_{S\phi}\varphi_S\varphi_\phi \\ \lambda_{S\phi}\varphi_S\varphi_\phi & 2\lambda_\phi\varphi_\phi^2 \end{pmatrix}, \tag{22}$$

whereas for the CP-odd scalar J and the Goldstone boson, it is

$$m_{J,{\rm GB}}^2(\varphi_S, \varphi_\phi) = \frac{\lambda_M\varphi_\phi}{2\sqrt{2}\Lambda}\begin{pmatrix} 9\varphi_S^2 & 6\varphi_S\varphi_\phi \\ 6\varphi_S\varphi_\phi & 4\varphi_\phi^2 \end{pmatrix}. \tag{23}$$

Assuming the quartic couplings are much smaller than the gauge coupling, which is precisely the parameter space region of interest for first order phase transitions, and choosing as a benchmark the new fermion $U(1)_\ell$ charges to be $\ell_1 = -1/2$ and $\ell_2 = 5/2$, the thermal mass for the gauge boson Z_ℓ is

$$\Pi_{Z_\ell}(T) = \frac{13}{2} g_\ell^2 T^2. \tag{24}$$

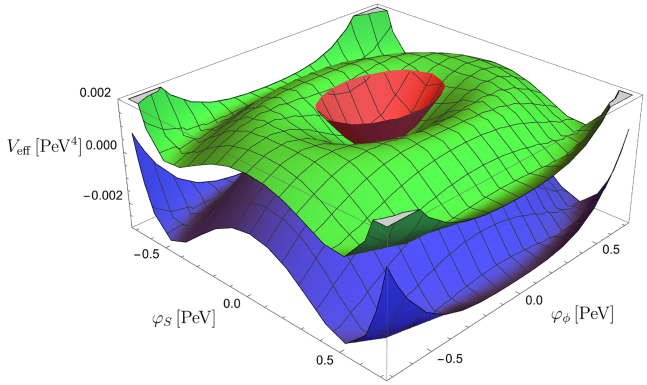

FIG. 1. Effective potential of the model $V_{\rm eff}(\varphi_S, \varphi_\phi, T)$ plotted for $v_S = v_\phi = 1$ PeV, $g_\ell = 0.6$, $\lambda_S = \lambda_\phi = 0.001$, $\lambda_{S\phi} = 0$, and the temperatures 450 TeV (blue), 550 TeV (green), 650 TeV (red).

For the *CP*-even scalars, as well as the *CP*-odd scalar and the Goldstone boson, the thermal mass matrices are the same and given by

$$\Pi_{\rm even}(T) = \Pi_{J,\rm GB}(T) = \frac{1}{4}\begin{pmatrix} 9 & 0 \\ 0 & 4 \end{pmatrix} g_\ell^2 T^2. \tag{25}$$

We find that for a wide range of quartic couplings and gauge couplings the effective potential develops vacua at nonzero field values which have a lower energy density than the high-temperature vacuum at $(\varphi_S, \varphi_\phi) = (0, 0)$, separated from each other by a potential bump. The new minima appear around the field values (v_S, v_ϕ), $(v_S, -v_\phi)$, $(-v_S, v_\phi)$, and $(-v_S, -v_\phi)$; however, two pairs of them are physically equivalent (for a related discussion in the more general case of a two Higgs doublet model, see [136,137]). In particular, since the effective potential is invariant under the $\mathcal{Z}_2$ transformation $\varphi_S \to -\varphi_S$, $\varphi_\phi \to \varphi_\phi$, just the two vacua around (v_S, v_ϕ) and $(v_S, -v_\phi)$ are physically distinct. Their energy densities differ only slightly due to the dimension-five term in Eq. (12). As will be discussed in Sec. V, this leads to the formation of domain walls, since the phase transition will populate both of those vacua.

Figure 1 shows a plot of the effective potential (prepared with *Mathematica* [138]) assuming the parameter values $v_S = v_\phi = 1$ PeV, $g_\ell = 0.6$, $\lambda_S = \lambda_\phi = 0.001$, and for several temperature values 450 TeV (blue), 550 TeV (green), and 650 TeV (red). For concreteness, we focus on a phase transition from the false vacuum (0, 0) to the true vacuum around (v_S, v_ϕ). Since the two vacua are separated by a potential bump, the transition will be first order, resulting in the formation of true vacuum bubbles in various patches of the Universe. If the conditions are right, those bubbles expand and eventually fill out the entire Universe.

The nucleation process can be initiated if the bubble nucleation rate becomes comparable to the Hubble expansion rate. This is described by the equation [139]

$$\left(\frac{S(T_*)}{2\pi T_*}\right)^{\frac{3}{2}} T_*^4 \exp\left(-\frac{S(T_*)}{T_*}\right) \approx H(T_*)^4, \tag{26}$$

where T_* is the nucleation temperature at which this happens, and $S(T)$ is the Euclidean action

$$S(T) = \int d^3x \left[\frac{1}{2}(\partial_\mu \vec{\varphi}_{\rm bubble})^2 + V_{\rm eff}(\vec{\varphi}_{\rm bubble}, T)\right]. \tag{27}$$

Here, $\vec{\varphi}_{\rm bubble}$ is the solution of the equation

$$\frac{d^2\vec{\varphi}}{dr^2} + \frac{2}{r}\frac{d\vec{\varphi}}{dr} - \vec{\nabla} V_{\rm eff}(\vec{\varphi}, T) = 0 \tag{28}$$

constrained by the two conditions

$$\left.\frac{d\vec{\varphi}}{dr}\right|_{r=0} = 0 \quad \text{and} \quad \vec{\varphi}(\infty) = \vec{\varphi}_{\rm false}. \tag{29}$$

Writing the Hubble constant in terms of the temperature, the Planck mass, and the number of active degrees of freedom,

$$H(T) \approx \frac{T^2}{M_P}\sqrt{\frac{4\pi^3 g_*}{45}}, \tag{30}$$

Eq. (26) takes the following form:

$$\frac{S(T_*)}{T_*} \approx \log\left(\frac{M_P^4}{T_*^4}\right) - \log\left[\left(\frac{4\pi^3 g_*}{45}\right)^2 \left(\frac{2\pi T_*}{S(T_*)}\right)^{\frac{3}{2}}\right]. \tag{31}$$

Upon finding the nucleation temperature from Eq. (31), one can calculate the other two model-dependent parameters describing the first order phase transition: the strength of the phase transition α and its duration $1/\tilde{\beta}$. The parameter α is given by the difference between the energy densities of the true and false vacuum divided by the energy density of radiation at the nucleation temperature,

$$\alpha = \frac{\Delta\rho_v(T_*)}{\frac{\pi^2}{30} g_* T_*^4}, \tag{32}$$

where the numerator is given by

$$\Delta\rho_v(T) = V_{\rm eff}(\vec{\varphi}_{\rm false}, T) - V_{\rm eff}(\vec{\varphi}_{\rm true}, T) - T\frac{\partial}{\partial T}[V_{\rm eff}(\vec{\varphi}_{\rm false}, T) - V_{\rm eff}(\vec{\varphi}_{\rm true}, T)]. \tag{33}$$

The parameter $\tilde{\beta}$ being the inverse of the duration of the phase transition is determined from

$$\tilde{\beta} = T_* \frac{d}{dT}\left(\frac{S(T)}{T}\right)\bigg|_{T=T_*}. \tag{34}$$

The dynamics of a first order phase transition also depends on the bubble wall velocity v_w. Here we assume that it is close to the speed of light, i.e., $v_w = c$. For the rationale behind other choices, see [140,141].

IV. GRAVITATIONAL WAVES FROM PHASE TRANSITION

As described in Sec. I, collisions between expanding bubbles, sound shock waves propagating through plasma, and magnetohydrodynamic turbulence generate a stochastic gravitational wave background permeating the Universe since then. The expectation regarding the shape of each contribution to the spectrum was derived from numerical simulations and the empirical formulas have been determined.

The contribution from bubbles collisions is [39,141–143]

$$h^2\Omega_{\rm coll}(\nu) \approx (4.9\times10^{-6})\frac{1}{\tilde{\beta}^2}\left(\frac{\kappa_c\alpha}{\alpha+1}\right)^2\left(\frac{100}{g_*}\right)^{\frac{1}{3}} \times \frac{\left(\frac{\nu}{\nu_c}\right)^{2.8}}{1+2.8\left(\frac{\nu}{\nu_c}\right)^{3.8}}, \tag{35}$$

where κ_c is the fraction of the latent heat deposited into the bubble front [144], and ν_c is the peak frequency,

$$\kappa_c = \frac{\frac{4}{27}\sqrt{\frac{3}{2}\alpha}+0.72\alpha}{1+0.72\alpha},$$
$$\nu_c = (0.037\ \text{Hz})\tilde{\beta}\left(\frac{g_*}{100}\right)^{\frac{1}{6}}\left(\frac{T_*}{1\ \text{PeV}}\right). \tag{36}$$

The sound wave contribution is given by [141,145]

$$h^2\Omega_{\rm sw}(\nu) \approx (1.9\times10^{-5})\frac{1}{\tilde{\beta}}\left(\frac{\kappa_s\alpha}{\alpha+1}\right)^2\left(\frac{100}{g_*}\right)^{\frac{1}{3}}\Upsilon \times \frac{\left(\frac{\nu}{\nu_s}\right)^3}{\left[1+0.75\left(\frac{\nu}{\nu_s}\right)^2\right]^{\frac{7}{2}}}, \tag{37}$$

where κ_s is the fraction of the latent heat going into the bulk motion of the plasma [140], ν_s is the peak frequency, and Υ is a suppression factor [146,147],

$$\kappa_s = \frac{\alpha}{0.73+0.083\sqrt{\alpha}+\alpha},$$
$$\nu_s = (0.19\ \text{Hz})\tilde{\beta}\left(\frac{g_*}{100}\right)^{\frac{1}{6}}\left(\frac{T_*}{1\ \text{PeV}}\right),$$
$$\Upsilon = 1-\left[1+\frac{8\sqrt{3}\pi}{\tilde{\beta}}\sqrt{\frac{\alpha+1}{3\kappa_s\alpha}}\right]^{-\frac{1}{2}}. \tag{38}$$

Magnetohydrodynamic turbulence results in [148,149]

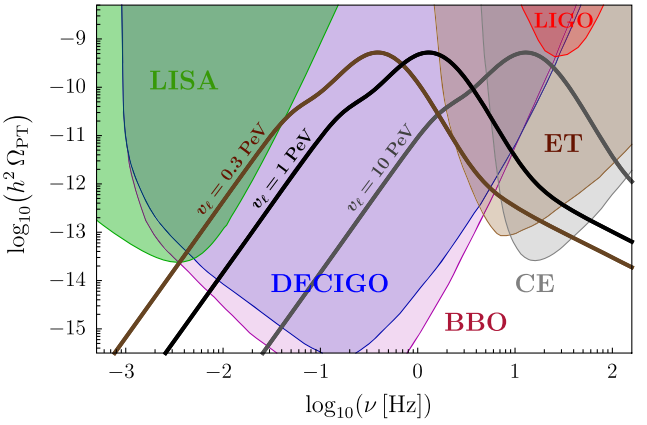

FIG. 2. First order phase-transition-generated stochastic gravitational wave background from $\mathrm{U}(1)_\ell$ breaking for the model parameters $g_\ell = 0.22$, $\lambda_S = \lambda_\phi \equiv \lambda = 10^{-4}$ at the phase transition, and for the three symmetry breaking scales 0.3 PeV (brown), 1 PeV (black), 10 PeV (gray). Sensitivities of future gravitational wave detectors LISA, DECIGO, BBO, ET, and CE, as well as the reach of LIGO's O5 observing run are shown as shaded regions.

$$h^2\Omega_{\rm turb}(\nu) \approx (3.4\times10^{-4})\frac{1}{\tilde{\beta}}\left(\frac{\epsilon\kappa_s\alpha}{\alpha+1}\right)^{\frac{3}{2}}\left(\frac{100}{g_*}\right)^{\frac{1}{3}} \times \frac{\left(\frac{\nu}{\nu_t}\right)^3}{\left(1+\frac{8\pi\nu}{h_*}\right)\left(1+\frac{\nu}{\nu_t}\right)^{\frac{11}{3}}}, \tag{39}$$

where we assumed $\epsilon = 0.05$ [141] and

$$\nu_t = (0.27\ \text{Hz})\tilde{\beta}\left(\frac{g_*}{100}\right)^{\frac{1}{6}}\left(\frac{T_*}{1\ \text{PeV}}\right),$$
$$h_* = (0.17\ \text{Hz})\left(\frac{g_*}{100}\right)^{\frac{1}{6}}\left(\frac{T_*}{1\ \text{PeV}}\right). \tag{40}$$

The total gravitational wave signal is

$$h^2\Omega_{\rm PT}(\nu) = h^2\Omega_{\rm sw}(\nu)+h^2\Omega_{\rm coll}(\nu)+h^2\Omega_{\rm turb}(\nu). \tag{41}$$

Figure 2 shows the gravitational wave spectrum of the model from a first order phase transition happening at three different symmetry breaking scales: v_ℓ= 0.3 PeV (brown curve), 1 PeV (black curve), and 10 PeV (gray curve). The signal was plotted using Eqs. (35)–(41), with the phase transition parameters calculated using Eqs. (26)–(34) for the gauge coupling $g_\ell = 0.22$, quartic couplings $\lambda_S = \lambda_\phi \equiv \lambda =$ 0.0001, and assuming that the mixed quartic coupling $\lambda_{S\phi}$ and the new fermion Yukawas are negligibly small. We note that the values of couplings were chosen at the scales of the phase transitions corresponding to the three representative curves in Fig. 2 independently; upon running the couplings, each curve corresponds to a different set of values for those couplings at a given energy scale.

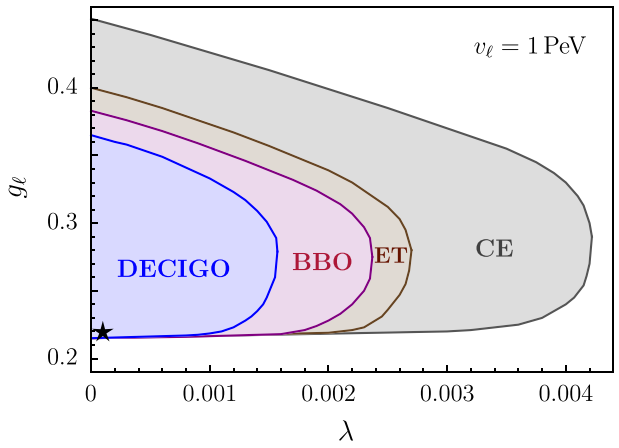

FIG. 3. Parameter space (λ, g_ℓ) for which a gravitational wave signal originating from a first order phase transition at the scale 1 PeV is within the reach of upcoming gravitational wave experiments (DECIGO, BBO, ET, CE) with a signal-to-noise ratio greater than 5. Colors for the various experiments are the same as in Fig. 2, and the star corresponds to the 1 PeV curve.

The strength of the phase transition and the inverse of its duration corresponding to the signals in Fig. 2 are $\alpha \approx 4$ and $\tilde{\beta} \approx 80$, whereas the nucleation temperatures are $T_* \approx 21$ TeV for the brown curve, $T_* \approx 70$ TeV for the black curve, and $T_* \approx 700$ TeV for the gray curve. For a given symmetry breaking scale, longer phase transitions (characterized by a smaller $\tilde{\beta}$) lead to stronger gravitational wave signals. The shape of the spectrum is dominated by the sound wave contribution in the central part, and by the bubble collision part at lower and at higher frequencies. The signal would be up to 2 orders of magnitude stronger if not for the sound wave suppression factor Υ in Eq. (37).

The shaded regions in Fig. 2 indicate the reach of several upcoming gravitational wave interferometers, including LISA [125] (green), DECIGO [123] (dark blue), Big Bang Observer [124] (magenta), Einstein Telescope [122] (brown), and Cosmic Explorer [121] (gray). The expected sensitivity of LIGO's O5 observing run [150] (red) is also included, but its reach is limited to theories with supercooled phase transitions, which is not the case for the model under consideration. For a symmetry breaking scale ∼PeV the signal is peaked around frequencies ∼1 Hz, and is within the reach of most of those detectors. As the scale of symmetry breaking decreases, the nucleation temperature T_* also decreases, and the peak of the spectrum moves to lower frequencies, eventually becoming searchable also in LISA when $v_\ell \lesssim 0.5$ PeV.

Figure 3 shows the region of parameter space of the quartic coupling λ versus the gauge coupling g_ℓ (assuming a symmetry breaking scale of $v_\ell = 1$ PeV) for which the model can be probed in future gravitational wave detectors. The colors of the shaded regions correspond to those in Fig. 2 for the various experiments. Not all parameters for which a first order phase transition occurs result in a measurable signal. The upper bound of the shaded regions corresponds to the signal being too weak to be detectable in any of the planned experiments (this includes the first order phase transition example shown in Fig. 1). On the other hand, parameter points below the shaded regions do not result in a first order phase transition at all, since the bubble nucleation rate never becomes comparable to the Hubble expansion rate.

V. DOMAIN WALLS

Given that the energy density splitting between the vacua (potential bias) located in the proximity of the field values (v_S, v_ϕ) and $(v_S, -v_\phi)$,

$$\Delta\rho = \frac{\lambda_M}{2\sqrt{2}\Lambda} v_S^2 v_\phi^3, \tag{42}$$

is small due to our assumption $\lambda_M/\Lambda \ll 1/v_S, 1/v_\phi$, the first order phase transition discussed in Sec. III populates both of them at similar rates. This creates domain walls, i.e., two-dimensional topological structures existing on the boundaries between the two vacua regions. Because of the nonzero energy density difference in Eq. (42), domain walls are unstable, and eventually undergo annihilation, avoiding the production of large density fluctuations in the Universe [105].

We denote the domain wall profile by $\vec{\phi}_{\mathrm{DW}}(z)$, where z is the axis perpendicular to the domain wall surface. It can be found as the solution of the following equation [96]:

$$\frac{d^2\vec{\varphi}_{\mathrm{DW}}(z)}{dz^2} - \vec{\nabla}_\phi V_{\mathrm{eff}}[\vec{\varphi}_{\mathrm{DW}}(z)] = 0, \tag{43}$$

with the boundary conditions,

$$\vec{\varphi}_{\mathrm{DW}}(-\infty) = (v_S, v_\phi), \qquad \vec{\varphi}_{\mathrm{DW}}(\infty) = (v_S, -v_\phi). \tag{44}$$

Apart from the potential bias $\Delta\rho$, domain walls are described also by the tension parameter σ defined as

$$\sigma = \int_{-\infty}^{\infty} dz \left[\frac{1}{2}\left(\frac{d\vec{\varphi}_{\mathrm{DW}}(z)}{dz}\right)^2 + V_{\mathrm{eff}}(\vec{\varphi}_{\mathrm{DW}}(z))\right]. \tag{45}$$

To a good approximation, one can write

$$\sigma \sim v_\ell^3. \tag{46}$$

Domain walls need to undergo efficient annihilation before they start dominating the energy density of the Universe. This is achieved by requiring

$$\Delta\rho > \frac{4C_{\mathrm{ann}}\mathcal{A}^2\sigma^2}{3M_P^2}, \tag{47}$$

where $C_{\rm ann}$ is a coefficient of $\mathcal{O}(1)$ and $\mathcal{A} \approx 0.8$ [105]. In our case, $v_S \sim v_\phi \sim 1$ PeV, and the above inequality is satisfied even for λ_M as small as 10^{-13} (since $\Lambda < M_P$). Another constraint on $\Delta\rho$ comes from the requirement of the domain walls annihilating before big bang nucleosynthesis, not to alter the ratios of the produced elements; however, that bound is weaker than the one in Eq. (47).

There is also an upper limit on the value of the potential bias resulting from the requirement of having sufficiently many patches of true and false vacua in the early Universe, so that the domain walls can actually be created. The corresponding condition is given by [105]

$$\Delta\rho < 0.795 V_0, \tag{48}$$

where V_0 is the difference between the values of the effective potential at the maximum and at the deeper minimum. For the values of the quartic couplings we consider, this condition is well satisfied in the entire region relevant for the upcoming gravitational wave experiments.

VI. GRAVITATIONAL WAVES FROM DOMAIN WALLS

Numerical simulations yield the following spectrum of the stochastic gravitational wave background generated by annihilating domain walls [93,105]:

$$h^2\Omega_{\rm DW}(\nu) \approx 7.1\times 10^{-33}\left(\frac{\sigma}{\rm PeV^2}\right)^4\left(\frac{\rm TeV^4}{\Delta\rho}\right)^2\left(\frac{100}{g_*}\right)^{\frac{1}{3}} \times\left[\left(\frac{\nu}{\nu_d}\right)^3\theta(\nu_d-\nu)+\left(\frac{\nu_d}{\nu}\right)\theta(\nu-\nu_d)\right]. \tag{49}$$

Here $\theta(\nu)$ is the Heaviside step function, $\mathcal{A} = 0.8$ was taken for the area parameter and $\tilde{\epsilon}_{\rm gw} = 0.7$ for the efficiency parameter [151], and ν_d is the signal's peak frequency given by

$$\nu_d \approx (0.14\ {\rm Hz})\sqrt{\left(\frac{\rm PeV^3}{\sigma}\right)\left(\frac{\Delta\rho}{\rm TeV^4}\right)}. \tag{50}$$

There is a constraint on the strength of the gravitational wave signal arising from cosmic microwave background measurements which requires $h^2\Omega(\nu) < 2.9\times 10^{-7}$ [152]. This translates to the condition

$$\sqrt{\Delta\rho} \gtrsim \frac{\sigma}{2.5\times 10^{12}\ {\rm PeV}}, \tag{51}$$

which is slightly stronger than the bound imposed by big bang nucleosynthesis in Eq. (47).

To investigate how this bound translates into constraints on the model parameters, in particular, the coefficient of the $\mathcal{Z}_2$ breaking term in Eq. (12), we rewrite Eq. (42) as

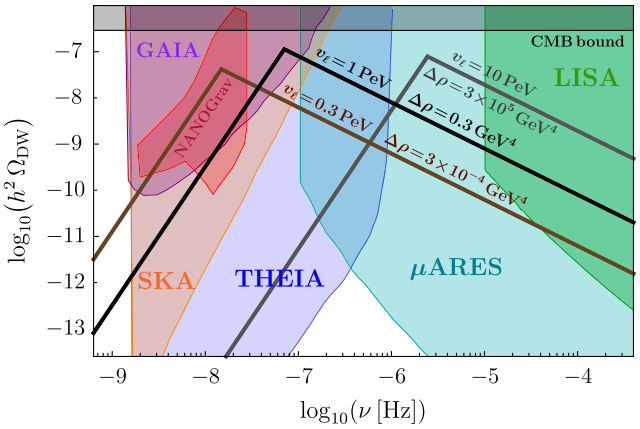

FIG. 4. Domain wall annihilation-induced stochastic gravitational wave background for several symmetry breaking scales 0.3 PeV (brown), 1 PeV (black), 10 PeV (gray), and the potential biases as described on the plot. Shaded regions depict the sensitivity of future gravitational wave and astrometry experiments.

$$\Delta\rho = \frac{\lambda_M}{2\sqrt{2}\Lambda} v_\ell^5 \sin^3(\xi)\cos^2(\xi), \tag{52}$$

where we parametrized $v_S \equiv v_\ell \cos(\xi)$ and $v_\phi \equiv v_\ell \sin(\xi)$, consistent with Eq. (10). Taking $v_\phi \ll v_S$, one obtains

$$\frac{\lambda_M}{\Lambda}\sin^3(\xi) \gtrsim \frac{v_\ell}{2.2\times 10^{24}\ {\rm PeV}^2}. \tag{53}$$

In Fig. 4. we included three representative signal curves for the stochastic gravitational wave background arising from domain wall annihilation, assuming the same choice of $U(1)_\ell$ breaking scales as for the phase transition case in Fig. 2, i.e., $v_\ell = 0.3$ PeV (brown curve), 1 PeV (black curve), and 10 PeV (gray curve). The adopted values for the potential bias, as indicated in the figure, are $\Delta\rho = 3\times 10^{-4}$ GeV^4, 0.3 GeV^4, and 3×10^5 GeV^4, respectively. As implied by the form of Eq. (49), at low frequencies the slope grows $\sim\nu^3$, whereas for high frequencies it falls $\sim 1/\nu$.

Overplotted in Fig. 4 as the shaded regions are the sensitivities of several upcoming experiments relevant for low-frequency gravitational wave search. This includes the planned space-based interferometers LISA [125] (green) and μARES [126] (cyan), the pulsar timing array SKA [128] (orange), and the astrometry experiments Theia [129] (light blue) and Gaia [130,131] (purple). We also indicated the region in which a stochastic gravitational wave signal has been observed by the NANOGrav experiment [127], and we find that the brown curve corresponding to $v_\ell = 0.3$ PeV and $\Delta\rho = 3\times 10^{-4}$ GeV^4 has the greatest overlap with the measured signal region.

Similar to the previous case, we performed a scan over $(v_\ell, \Delta\rho)$ and determined the parameter space regions which yield measurable signals in the experiments listed above;

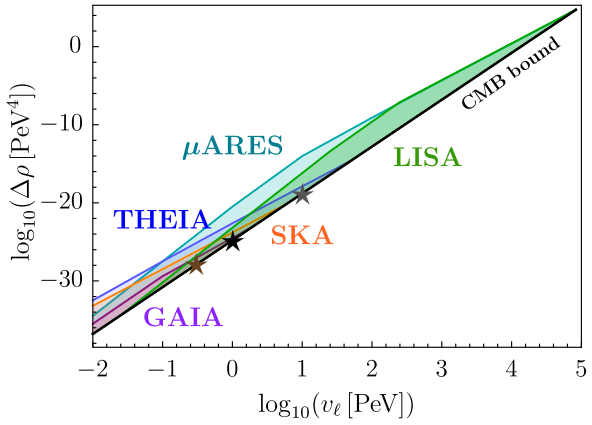

FIG. 5. Regions of parameter space $(v_\ell, \Delta\rho)$ with a signal-to-noise ratio of the gravitational wave signature generated by domain wall annihilation greater than 5 in various experiments. The choice of colors matches that in Fig. 4, and the stars correspond to the three curves for $v_\ell = 0.3$, 1, 10 PeV.

the results are shown in Fig. 5. The lower bound depicted by the black line corresponds to the cosmic microwave background constraint given by Eq. (51). The colors chosen for various experiments correspond to the ones used in Fig. 4.

We emphasize that the results shown in Fig. 5 are model independent and can be applied to any theory with a domain wall gravitational wave signature. Those results are therefore complementary to the model-independent constraints on the domain wall parameters $(v, \Delta\rho)$ derived in [87] (see Fig. 4 in that reference) derived for higher symmetry breaking scales relevant for DECIGO, BBO, ET, and CE.

Finally, those constraints can be translated into bounds on the coefficient of the $\mathcal{Z}_2$ breaking dimension-five term. For example, assuming $v_S \sim 10$ PeV and $v_\phi \sim 1$ TeV (for the seesaw mechanism, this requires $y_\nu \sim 10^{-6}$), the μARES experiment will be able to test the parameter region

$$4 \times 10^6 \text{ PeV} \lesssim \frac{\Lambda}{\lambda_M} \lesssim 2 \times 10^{11} \text{ PeV}, \tag{54}$$

providing the opportunity to probe the scale of new physics responsible for the generation of the higher-dimensional term in Eq. (12) using gravitational waves.

VII. GRAVITATIONAL WAVE SPECTRUM OF THE MODEL

Since the gauged lepton number breaking in the model leads to a first order phase transition with the formation of domain walls, which subsequently annihilate, this results in a unique gravitational wave signature involving a domain wall peak at lower frequencies and a phase transition bump at higher frequencies. If the $\mathrm{U}(1)_\ell$ breaking occurs at ∼PeV, this signature can be searched for in most of the upcoming experiments sensitive to gravitational waves. This is demonstrated in Fig. 6, which shows the signal expected from the model if the gauged lepton number symmetry is broken at the scale $v_\ell = 1$ PeV, and assuming the gauge coupling $g_\ell = 0.22$, the quartic couplings $\lambda_S = \lambda_\phi = 10^{-4}$, and the potential bias $\Delta\rho = 0.6$ GeV^4.

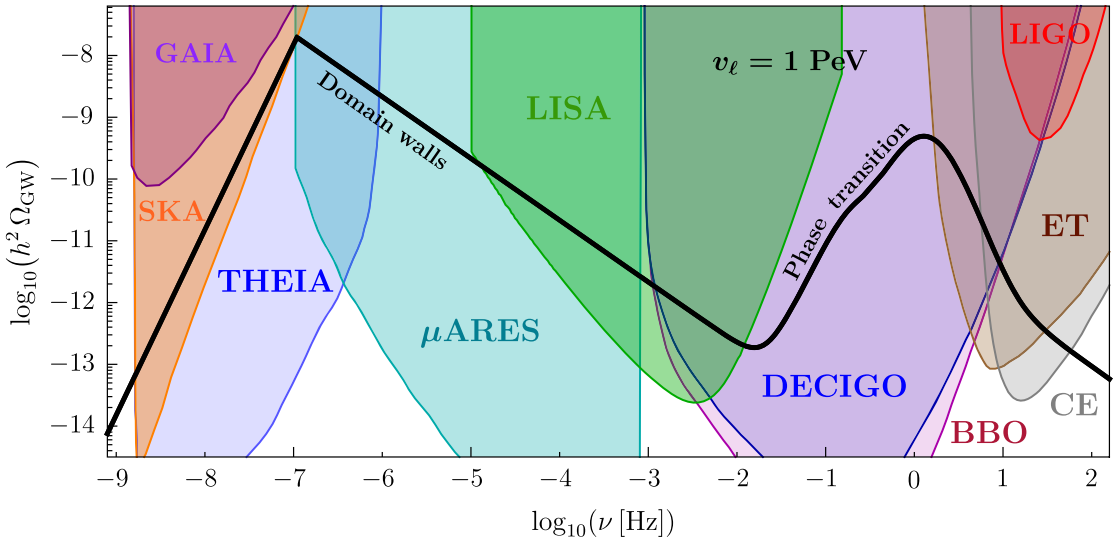

FIG. 6. Gravitational wave signature of the model with gauged lepton number broken at the scale $v_\ell = 1$ PeV. The domain wall contribution at low frequencies is plotted assuming a potential bias of $\Delta\rho = 0.6$ GeV^4, whereas the high-frequency first order phase transition part corresponds to the choice of the gauge coupling $g_\ell = 0.22$ and the quartic couplings $\lambda_S = \lambda_\phi = 0.0001$. The sensitivity reach of future experiments is shown as the shaded regions, which include GAIA [130,131] (purple), SKA [128] (orange), THEIA [129] (light blue), μARES [126] (cyan), LISA [125] (green), DECIGO [123](dark blue), Big Bang Observer [124] (magenta), Einstein Telescope [122] (brown), Cosmic Explorer [121] (gray), and LIGO after the O5 observing run [150] (red).

As visible in the plot, this signal can be searched for at low frequencies in the upcoming pulsar timing array SKA [128] (orange region), astrometry experiment Theia [129] (light blue region), space-based interferometer μARES [126] (cyan), throughout intermediate frequencies at gravitational wave interferometers LISA [125] (green), DECIGO [123] (dark blue) and Big Bang Observer [124] (magenta), and up to high frequencies at the Einstein Telescope [122] (brown) and Cosmic Explorer [121] (gray). We note that for lower symmetry breaking scales the domain wall signal may be searchable at the astrometry experiment Gaia [130,131] (purple), but the phase transition contribution is too weak to be detectable by LIGO [150] (red) even after its O5 observing run.

Given the difference in slope of the domain wall and phase transition contributions, the two can be distinguished. The domain wall spectrum dependence on frequency is $\sim\nu^3$ to the left of the peak and $\sim 1/\nu$ to the right. For the phase transition spectrum the dependence is $\sim\nu^{2.8}$ at low frequencies where the bubble collision contribution dominates, $\sim\nu^3$ just to the left, and $\sim 1/\nu^4$ just to the right of the peak from the sound wave contribution, turning into $\sim 1/\nu$ at higher frequencies again from the bubble collision contribution. There is also a nontrivial dependence on frequency where the two peaks meet, which can be investigated by DECIGO and BBO.

It is quite remarkable that a single symmetry breaking leads to a signature that is searchable both at pulsar timing arrays and at gravitational wave interferometers. In case it is seen in one of the detectors, this scenario will foster collaboration between the different experimental groups, since only their combined efforts would lead to determining the full spectrum of the model.

VIII. SUMMARY

Despite the huge experimental effort to discover beyond-Standard-Model physics at the Large Hadron Collider, in dark matter direct detection experiments, and through indirect detection observations, so far no indisputable evidence of new physics has been found. This prompted particle physics to look for synergies with other areas of physics and expand its search strategies, especially since the guidance from theory is clear—new particles and phenomena are needed to explain the outstanding open questions, such as the nature of dark matter, the origin of the matter-antimatter asymmetry, or the mechanism behind neutrino masses. One such promising synergy has arisen after the first direct detection of gravitational waves by LIGO. A potential discovery of a primordial gravitational wave background from the early Universe would certainly initiate a new golden age for particle physics.

Among processes producing stochastic gravitational wave signals are first order phase transitions and domain wall annihilation in the early Universe. From a theoretical perspective, they arise when one or more symmetries of the theory are spontaneously broken and the vacuum state abruptly changes. The expected shape of the gravitational wave spectrum was determined via simulations and is relatively well understood. Thus far, in the models considered in the literature, each gauge symmetry breaking led to just a single feature in the gravitational wave spectrum which would be within the reach of upcoming experiments. The cases where several measurable features were present in the spectrum required the breaking of two or more gauge groups.

The uniqueness of the model considered here arises from its prediction of two types of gravitational wave contributions from just a single gauge symmetry breaking. This leads to gravitational wave signatures with a double-peaked spectrum, consisting of a domain-wall-induced peak at low frequencies and a peak from phase transitions at high frequencies, with the former searchable mainly in pulsar timing arrays and through astrometry measurements, while the latter in interferometers. Since both peaks originate from the breaking of the same gauge group, the domain wall contribution is necessarily shifted to lower frequencies compared to the phase transition one. As mentioned above, this feature differentiates the model from other theories in which, although both such peaks also exist in the spectrum [86,87], two separate gauge symmetries have to be broken for the signature to take this shape. An additional difference is that in these other models, in contrast to the predictions of the model considered in this paper, the domain wall peak appears at higher frequencies than the first order phase transition peak.

A natural extension of the model would be to introduce a gauged baryon number symmetry $\mathrm{U}(1)_B$ broken at a higher energy scale. This would make the model even more attractive, not only accommodating a low-scale seesaw for neutrino masses and a dark matter candidate, but also explaining the matter-antimatter asymmetry through high-scale baryogenesis. This could result in the appearance of an additional feature in the gravitational wave spectrum, such as a cosmic string contribution or an extra domain wall peak at higher frequencies. Apart from that, it would also be intriguing to build an explicit UV completion for the $\mathcal{Z}_2$ breaking dimension-five term, offering additional insight into the particle physics origins of the domain wall signal.

ACKNOWLEDGMENTS

This research was supported by the National Science Foundation under Grant No. PHY-2213144.

[1] S. L. Glashow, Partial symmetries of weak interactions, Nucl. Phys. **22**, 579 (1961).
[2] P. W. Higgs, Broken symmetries and the masses of gauge bosons, Phys. Rev. Lett. **13**, 508 (1964).
[3] F. Englert and R. Brout, Broken symmetry and the mass of gauge vector mesons, Phys. Rev. Lett. **13**, 321 (1964).
[4] S. Weinberg, A model of leptons, Phys. Rev. Lett. **19**, 1264 (1967).
[5] A. Salam, Weak and electromagnetic interactions, Conf. Proc. C **680519**, 367 (1968).
[6] H. Fritzsch, M. Gell-Mann, and H. Leutwyler, Advantages of the color octet gluon picture, Phys. Lett. **47B**, 365 (1973).
[7] D. J. Gross and F. Wilczek, Ultraviolet behavior of non-Abelian gauge theories, Phys. Rev. Lett. **30**, 1343 (1973).
[8] H. D. Politzer, Reliable perturbative results for strong interactions?, Phys. Rev. Lett. **30**, 1346 (1973).
[9] V. C. Rubin and W. K. Ford, Jr., Rotation of the Andromeda Nebula from a spectroscopic survey of emission regions, Astrophys. J. **159**, 379 (1970).
[10] P. de Bernardis *et al.* (Boomerang Collaboration), A flat universe from high resolution maps of the cosmic microwave background radiation, Nature (London) **404**, 955 (2000).
[11] R. Gavazzi, T. Treu, J. D. Rhodes, L. V. Koopmans, A. S. Bolton, S. Burles, R. Massey, and L. A. Moustakas, The Sloan Lens ACS Survey. 4. The mass density profile of early-type galaxies out to 100 effective radii, Astrophys. J. **667**, 176 (2007).
[12] P. Minkowski, $\mu \to e\gamma$ at a rate of one out of 10^9 muon decays?, Phys. Lett. **67B**, 421 (1977).
[13] M. Gell-Mann, P. Ramond, and R. Slansky, in *Supergravity*, edited by P. van Nieuwenhuizen and D. Freedman (North Holland, Amsterdam, 1979), pp. 315–321.
[14] T. Yanagida, Horizontal gauge symmetry and masses of neutrinos, Conf. Proc. C **7902131**, 95 (1979).
[15] R. N. Mohapatra and G. Senjanovic, Neutrino mass and spontaneous parity nonconservation, Phys. Rev. Lett. **44**, 912 (1980).
[16] W. Konetschny and W. Kummer, Nonconservation of total lepton number with scalar bosons, Phys. Lett. **70B**, 433 (1977).
[17] J. Schechter and J. W. F. Valle, Neutrino masses in $\mathrm{SU}(2) \times \mathrm{U}(1)$ theories, Phys. Rev. D **22**, 2227 (1980).
[18] T. P. Cheng and Ling-Fong Li, Neutrino masses, mixings, and oscillations in $\mathrm{SU}(2) \times \mathrm{U}(1)$ models of electroweak interactions, Phys. Rev. D **22**, 2860 (1980).
[19] R. N. Mohapatra and G. Senjanovic, Neutrino masses and mixings in gauge models with spontaneous parity violation, Phys. Rev. D **23**, 165 (1981).
[20] R. Foot, H. Lew, X. G. He, and G. C. Joshi, Seesaw neutrino masses induced by a triplet of leptons, Z. Phys. C **44**, 441 (1989).
[21] A. Zee, A theory of lepton number violation, neutrino Majorana mass, and oscillation, Phys. Lett. **93B**, 389 (1980); **95B**, 461(E) (1980).
[22] A. Pais, Remark on baryon conservation, Phys. Rev. D **8**, 1844 (1973).
[23] S. Rajpoot, Gauge symmetries of electroweak interactions, Int. J. Theor. Phys. **27**, 689 (1988).
[24] R. Foot, G. C. Joshi, and H. Lew, Gauged baryon and lepton numbers, Phys. Rev. D **40**, 2487 (1989).
[25] C. D. Carone and H. Murayama, Realistic models with a light $U(1)$ gauge boson coupled to baryon number, Phys. Rev. D **52**, 484 (1995).
[26] H. Georgi and S. L. Glashow, Decays of a leptophobic gauge boson, Phys. Lett. B **387**, 341 (1996).
[27] P. Fileviez Perez and M. B. Wise, Baryon and lepton number as local gauge symmetries, Phys. Rev. D **82**, 011901 (2010); **82**, 079901(E) (2010).
[28] M. Duerr, P. Fileviez Perez, and M. B. Wise, Gauge theory for baryon and lepton numbers with leptoquarks, Phys. Rev. Lett. **110**, 231801 (2013).
[29] P. Fileviez Perez, S. Ohmer, and H. H. Patel, Minimal theory for lepto-baryons, Phys. Lett. B **735**, 283 (2014).
[30] J. M. Arnold, P. Fileviez Perez, B. Fornal, and S. Spinner, B and L at the supersymmetry scale, dark matter, and R-parity violation, Phys. Rev. D **88**, 115009 (2013).
[31] B. Fornal, A. Rajaraman, and T. M. P. Tait, Baryon number as the fourth color, Phys. Rev. D **92**, 055022 (2015).
[32] B. Fornal and T. M. P. Tait, Dark matter from unification of color and baryon number, Phys. Rev. D **93**, 075010 (2016).
[33] B. Fornal, Y. Shirman, T. M. P. Tait, and J. Rittenhouse West, Asymmetric dark matter and baryogenesis from $SU(2)_\ell$, Phys. Rev. D **96**, 035001 (2017).
[34] M. Duerr and P. Fileviez Perez, Theory for baryon number and dark matter at the LHC, Phys. Rev. D **91**, 095001 (2015).
[35] S. Ohmer and H. H. Patel, Leptobaryons as Majorana dark matter, Phys. Rev. D **92**, 055020 (2015).
[36] P. Fileviez Perez, E. Golias, R.-H. Li, and C. Murgui, Leptophobic dark matter and the baryon number violation scale, Phys. Rev. D **99**, 035009 (2019).
[37] P. Fileviez Perez, C. Murgui, and A. D. Plascencia, Baryogenesis via leptogenesis: Spontaneous B and L violation, Phys. Rev. D **104**, 055007 (2021).
[38] B. P. Abbott *et al.* (LIGO Scientific and Virgo Collaborations), Observation of gravitational waves from a binary black hole merger, Phys. Rev. Lett. **116**, 061102 (2016).
[39] A. Kosowsky, M. S. Turner, and R. Watkins, Gravitational radiation from colliding vacuum bubbles, Phys. Rev. D **45**, 4514 (1992).
[40] T. Vachaspati and A. Vilenkin, Gravitational radiation from cosmic strings, Phys. Rev. D **31**, 3052 (1985).
[41] M. Sakellariadou, Gravitational waves emitted from infinite strings, Phys. Rev. D **42**, 354 (1990); **43**, 4150(E) (1991).
[42] T. Hiramatsu, M. Kawasaki, and K. Saikawa, Gravitational waves from collapsing domain walls, J. Cosmol. Astropart. Phys. 05 (2010) 032.
[43] M. S. Turner, Detectability of inflation produced gravitational waves, Phys. Rev. D **55**, R435 (1997).
[44] C. Grojean and G. Servant, Gravitational waves from phase transitions at the electroweak scale and beyond, Phys. Rev. D **75**, 043507 (2007).
[45] P. Schwaller, Gravitational waves from a dark phase transition, Phys. Rev. Lett. **115**, 181101 (2015).
[46] V. Vaskonen, Electroweak baryogenesis and gravitational waves from a real scalar singlet, Phys. Rev. D **95**, 123515 (2017).

[47] G. C. Dorsch, S. J. Huber, T. Konstandin, and J. M. No, A second Higgs doublet in the early universe: Baryogenesis and gravitational waves, J. Cosmol. Astropart. Phys. 05 (2017) 052.
[48] I. Baldes, Gravitational waves from the asymmetric-dark-matter generating phase transition, J. Cosmol. Astropart. Phys. 05 (2017) 028.
[49] J. Bernon, L. Bian, and Y. Jiang, A new insight into the phase transition in the early universe with two Higgs doublets, J. High Energy Phys. 05 (2018) 151.
[50] M. Chala, C. Krause, and G. Nardini, Signals of the electroweak phase transition at colliders and gravitational wave observatories, J. High Energy Phys. 07 (2018) 062.
[51] A. Angelescu and P. Huang, Multistep strongly first order phase transitions from new fermions at the TeV scale, Phys. Rev. D **99**, 055023 (2019).
[52] V. Brdar, A. J. Helmboldt, and J. Kubo, Gravitational waves from first-order phase transitions: LIGO as a window to unexplored seesaw scales, J. Cosmol. Astropart. Phys. 02 (2019) 021.
[53] N. Okada and O. Seto, Probing the seesaw scale with gravitational waves, Phys. Rev. D **98**, 063532 (2018).
[54] D. Croon, T. E. Gonzalo, and G. White, Gravitational waves from a Pati-Salam phase transition, J. High Energy Phys. 02 (2019) 083.
[55] A. Alves, T. Ghosh, H.-K. Guo, K. Sinha, and D. Vagie, Collider and gravitational wave complementarity in exploring the singlet extension of the standard model, J. High Energy Phys. 04 (2019) 052.
[56] M. Breitbach, J. Kopp, E. Madge, T. Opferkuch, and P. Schwaller, Dark, cold, and noisy: Constraining secluded hidden sectors with gravitational waves, J. Cosmol. Astropart. Phys. 07 (2019) 007.
[57] D. Croon, V. Sanz, and G. White, Model discrimination in gravitational wave spectra from dark phase transitions, J. High Energy Phys. 08 (2018) 203.
[58] E. Hall, T. Konstandin, R. McGehee, H. Murayama, and G. Servant, Baryogenesis from a dark first-order phase transition, J. High Energy Phys. 04 (2020) 042.
[59] J. Ellis, M. Lewicki, J. M. No, and V. Vaskonen, Gravitational wave energy budget in strongly supercooled phase transitions, J. Cosmol. Astropart. Phys. 06 (2019) 024.
[60] P. S. B. Dev, F. Ferrer, Y. Zhang, and Y. Zhang, Gravitational waves from first-order phase transition in a simple axion-like particle model, J. Cosmol. Astropart. Phys. 11 (2019) 006.
[61] T. Hasegawa, N. Okada, and O. Seto, Gravitational waves from the minimal gauged $U(1)_{B-L}$ model, Phys. Rev. D **99**, 095039 (2019).
[62] B. Von Harling, A. Pomarol, O. Pujolas, and F. Rompineve, Peccei-Quinn phase transition at LIGO, J. High Energy Phys. 04 (2020) 195.
[63] L. Delle Rose, G. Panico, M. Redi, and A. Tesi, Gravitational waves from supercool axions, J. High Energy Phys. 04 (2020) 025.
[64] M. Lewicki and V. Vaskonen, On bubble collisions in strongly supercooled phase transitions, Phys. Dark Universe **30**, 100672 (2020).
[65] A. Greljo, T. Opferkuch, and B. A. Stefanek, Gravitational imprints of flavor hierarchies, Phys. Rev. Lett. **124**, 171802 (2020).
[66] W.-C. Huang, F. Sannino, and Z.-W. Wang, Gravitational waves from Pati-Salam dynamics, Phys. Rev. D **102**, 095025 (2020).
[67] N. Okada, O. Seto, and H. Uchida, Gravitational waves from breaking of an extra $U(1)$ in $SO(10)$ grand unification, Prog. Theor. Exp. Phys. **2021**, 033B01 (2021).
[68] M. Lewicki and V. Vaskonen, Gravitational wave spectra from strongly supercooled phase transitions, Eur. Phys. J. C **80**, 1003 (2020).
[69] J. Ellis, M. Lewicki, and V. Vaskonen, Updated predictions for gravitational waves produced in a strongly supercooled phase transition, J. Cosmol. Astropart. Phys. 11 (2020) 020.
[70] B. Fornal and B. Shams Es Haghi, Baryon and lepton number violation from gravitational waves, Phys. Rev. D **102**, 115037 (2020).
[71] X.-F. Han, L. Wang, and Y. Zhang, Dark matter, electroweak phase transition, and gravitational waves in the type II two-Higgs-doublet model with a singlet scalar field, Phys. Rev. D **103**, 035012 (2021).
[72] B. Fornal, Gravitational wave signatures of lepton universality violation, Phys. Rev. D **103**, 015018 (2021).
[73] N. Craig, N. Levi, A. Mariotti, and D. Redigolo, Ripples in spacetime from broken supersymmetry, J. High Energy Phys. 02 (2020) 184.
[74] B. Fornal, B. Shams Es Haghi, J.-H. Yu, and Y. Zhao, Gravitational waves from mini-split SUSY, Phys. Rev. D **104**, 115005 (2021).
[75] P. Di Bari, D. Marfatia, and Y.-L. Zhou, Gravitational waves from first-order phase transitions in Majoron models of neutrino mass, J. High Energy Phys. 10 (2021) 193.
[76] A. Azatov, M. Vanvlasselaer, and W. Yin, Dark matter production from relativistic bubble walls, J. High Energy Phys. 03 (2021) 288.
[77] R. Zhou, L. Bian, and Y. Du, Electroweak phase transition and gravitational waves in the type-II seesaw model, J. High Energy Phys. 08 (2022) 205.
[78] N. Benincasa, L. Delle Rose, K. Kannike, and L. Marzola, Multistep phase transitions and gravitational waves in the inert doublet model, J. Cosmol. Astropart. Phys. 12 (2022) 025.
[79] K. Kawana, Cosmology of a supercooled universe, Phys. Rev. D **105**, 103515 (2022).
[80] F. Costa, S. Khan, and J. Kim, A two-component dark matter model and its associated gravitational waves, J. High Energy Phys. 06 (2022) 026.
[81] B. Fu and S. F. King, Gravitational wave signals from leptoquark-induced first-order electroweak phase transitions, J. Cosmol. Astropart. Phys. 05 (2023) 055.
[82] F. Costa, S. Khan, and J. Kim, A two-component vector WIMP—fermion FIMP dark matter model with an extended seesaw mechanism, J. High Energy Phys. 12 (2022) 165.
[83] B. Fornal and E. Pierre, Asymmetric dark matter from gravitational waves, Phys. Rev. D **106**, 115040 (2022).

[84] M. Kierkla, A. Karam, and B. Swiezewska, Conformal model for gravitational waves and dark matter: A status update, J. High Energy Phys. 03 (2023) 007.
[85] A. Azatov, G. Barni, S. Chakraborty, M. Vanvlasselaer, and W. Yin, Ultra-relativistic bubbles from the simplest Higgs portal and their cosmological consequences, J. High Energy Phys. 10 (2022) 017.
[86] B. Fornal, K. Garcia, and E. Pierre, Testing unification and dark matter with gravitational waves, Phys. Rev. D **108**, 055022 (2023).
[87] J. Bosch, Z. Delgado, B. Fornal, and A. Leon, Gravitational wave signatures of gauged baryon and lepton number, Phys. Rev. D **108**, 095014 (2023).
[88] N. Bunji, B. Fornal, and K. Garcia, Shedding light on dark sectors with gravitational waves, Phys. Rev. D **110**, 075030 (2024).
[89] R. Caldwell *et al.*, Detection of early-universe gravitational-wave signatures and fundamental physics, Gen. Relativ. Gravit. **54**, 156 (2022).
[90] P. Athron, C. Balazs, A. Fowlie, L. Morris, and L. Wu, Cosmological phase transitions: From perturbative particle physics to gravitational waves, Prog. Part. Nucl. Phys. **135**, 104094 (2024).
[91] R. Roshan and G. White, Using gravitational waves to see the first second of the Universe, arXiv:2401.04388.
[92] C. Badger, B. Fornal, K. Martinovic, A. Romero, K. Turbang, H. Guo, A. Mariotti, M. Sakellariadou, A. Sevrin, F.-W. Yang, and Y. Zhao, Probing early universe supercooled phase transitions with gravitational wave data, Phys. Rev. D **107**, 023511 (2023).
[93] K. Kadota, M. Kawasaki, and K. Saikawa, Gravitational waves from domain walls in the next-to-minimal supersymmetric standard model, J. Cosmol. Astropart. Phys. 10 (2015) 041.
[94] M. Eto, M. Kurachi, and M. Nitta, Constraints on two Higgs doublet models from domain walls, Phys. Lett. B **785**, 447 (2018).
[95] M. Eto, M. Kurachi, and M. Nitta, Non-Abelian strings and domain walls in two Higgs doublet models, J. High Energy Phys. 08 (2018) 195.
[96] N. Chen, T. Li, Z. Teng, and Y. Wu, Collapsing domain walls in the two-Higgs-doublet model and deep insights from the EDM, J. High Energy Phys. 10 (2020) 081.
[97] R. A. Battye, A. Pilaftsis, and D. G. Viatic, Domain wall constraints on two-Higgs-doublet models with Z_2 symmetry, Phys. Rev. D **102**, 123536 (2020).
[98] N. Craig, I. Garcia Garcia, G. Koszegi, and A. McCune, P not PQ, J. High Energy Phys. 09 (2021) 130.
[99] D. I. Dunsky, A. Ghoshal, H. Murayama, Y. Sakakihara, and G. White, GUTs, hybrid topological defects, and gravitational waves, Phys. Rev. D **106**, 075030 (2022).
[100] S. Blasi, A. Mariotti, A. Rase, A. Sevrin, and K. Turbang, Friction on ALP domain walls and gravitational waves, J. Cosmol. Astropart. Phys. 04 (2023) 008.
[101] A. Chatterjee, A. Datta, and S. Roy, Electroweak phase transition in the Z_3-invariant NMSSM: Implications of LHC and dark matter searches and prospects of detecting the gravitational waves, J. High Energy Phys. 06 (2022) 108.
[102] B. Barman, D. Borah, A. Dasgupta, and A. Ghoshal, Probing high scale Dirac leptogenesis via gravitational waves from domain walls, Phys. Rev. D **106**, 015007 (2022).
[103] D. Borah and A. Dasgupta, Probing left-right symmetry via gravitational waves from domain walls, Phys. Rev. D **106**, 035016 (2022).
[104] S. F. King, D. Marfatia, and M. H. Rahat, Toward distinguishing Dirac from Majorana neutrino mass with gravitational waves, Phys. Rev. D **109**, 035014 (2024).
[105] K. Saikawa, A review of gravitational waves from cosmic domain walls, Universe **3**, 40 (2017).
[106] Y. Jiang and Q.-G. Huang, Implications for cosmic domain walls from the first three observing runs of LIGO-Virgo, Phys. Rev. D **106**, 103036 (2022).
[107] J. J. Blanco-Pillado and K. D. Olum, Stochastic gravitational wave background from smoothed cosmic string loops, Phys. Rev. D **96**, 104046 (2017).
[108] C. Ringeval and T. Suyama, Stochastic gravitational waves from cosmic string loops in scaling, J. Cosmol. Astropart. Phys. 12 (2017) 027.
[109] Y. Cui, M. Lewicki, D. E. Morrissey, and J. D. Wells, Cosmic archaeology with gravitational waves from cosmic strings, Phys. Rev. D **97**, 123505 (2018).
[110] Y. Cui, M. Lewicki, D. E. Morrissey, and J. D. Wells, Probing the pre-BBN universe with gravitational waves from cosmic strings, J. High Energy Phys. 01 (2019) 081.
[111] G. S. F. Guedes, P. P. Avelino, and L. Sousa, Signature of inflation in the stochastic gravitational wave background generated by cosmic string networks, Phys. Rev. D **98**, 123505 (2018).
[112] J. A. Dror, T. Hiramatsu, K. Kohri, H. Murayama, and G. White, Testing the seesaw mechanism and leptogenesis with gravitational waves, Phys. Rev. Lett. **124**, 041804 (2020).
[113] Y. Gouttenoire, G. Servant, and P. Simakachorn, BSM with cosmic strings: Heavy, up to EeV mass, unstable particles, J. Cosmol. Astropart. Phys. 07 (2020) 016.
[114] W. Buchmuller, V. Domcke, H. Murayama, and K. Schmitz, Probing the scale of grand unification with gravitational waves, Phys. Lett. B **809**, 135764 (2020).
[115] Stephen F. King, Silvia Pascoli, Jessica Turner, and Ye-Ling Zhou, Gravitational waves and proton decay: Complementary windows into grand unified theories, Phys. Rev. Lett. **126**, 021802 (2021).
[116] P. Ghosh, T. Ghosh, and S. Roy, Interplay among gravitational waves, dark matter and collider signals in the singlet scalar extended type-II seesaw model, J. High Energy Phys. 10 (2023) 057.
[117] B. Fu, A. Ghoshal, and S. F. King, Cosmic string gravitational waves from global $U(1)_{B-L}$ symmetry breaking as a probe of the type I seesaw scale, J. High Energy Phys. 11 (2023) 071.
[118] Y. Gouttenoire, G. Servant, and P. Simakachorn, Beyond the standard models with cosmic strings, J. Cosmol. Astropart. Phys. 07 (2020) 032.
[119] R. Abbott *et al.* (LIGO Scientific, Virgo, and KAGRA Collaborations), Constraints on cosmic strings using data from the third Advanced LIGO–Virgo observing run, Phys. Rev. Lett. **126**, 241102 (2021).

[120] H. Debnath and P. Fileviez Perez, Low scale seesaw mechanism with local lepton number, Phys. Rev. D **108**, 075009 (2023).
[121] D. Reitze *et al.*, Cosmic Explorer: The U.S. contribution to gravitational-wave astronomy beyond LIGO, Bull. Am. Astron. Soc. **51**, 035 (2019), https://baas.aas.org/pub/2020n7i035/release/1.
[122] M. Punturo *et al.*, The Einstein Telescope: A third-generation gravitational wave observatory, Classical Quantum Gravity **27**, 194002 (2010).
[123] S. Kawamura *et al.*, The Japanese space gravitational wave antenna: DECIGO, Classical Quantum Gravity **28**, 094011 (2011).
[124] J. Crowder and N. J. Cornish, Beyond LISA: Exploring future gravitational wave missions, Phys. Rev. D **72**, 083005 (2005).
[125] P. Amaro-Seoane *et al.* (LISA Collaboration), Laser Interferometer Space Antenna, arXiv:1702.00786.
[126] Alberto Sesana *et al.*, Unveiling the gravitational universe at μ-Hz frequencies, Exp. Astron. **51**, 1333 (2021).
[127] Z. Arzoumanian *et al.* (NANOGRAV Collaboration), The NANOGrav 11-year data set: Pulsar-timing constraints on the stochastic gravitational-wave background, Astrophys. J. **859**, 47 (2018).
[128] A. Weltman *et al.*, Fundamental physics with the square kilometre array, Pub. Astron. Soc. Aust. **37**, e002 (2020).
[129] Juan Garcia-Bellido, Hitoshi Murayama, and Graham White, Exploring the early universe with Gaia and Theia, J. Cosmol. Astropart. Phys. 12 (2021) 023.
[130] A. G. A. Brown *et al.* (Gaia Collaboration), Gaia Data Release 2. Summary of the contents and survey properties, Astron. Astrophys. **616**, A1 (2018).
[131] C. J. Moore, D. P. Mihaylov, A. Lasenby, and G. Gilmore, Astrometric search method for individually resolvable gravitational wave sources with Gaia, Phys. Rev. Lett. **119**, 261102 (2017).
[132] J. Heeck and H. H. Patel, Majoron at two loops, Phys. Rev. D **100**, 095015 (2019).
[133] N. Aghanim *et al.* (Planck Collaboration), Planck 2018 results. VI. Cosmological parameters, Astron. Astrophys. **641**, A6 (2020); **652**, C4(E) (2021).
[134] M. Quiros, Finite temperature field theory and phase transitions, in *Proceedings of the ICTP Summer School in High-Energy Physics and Cosmology*, arXiv:hep-ph/9901312.
[135] J. M. Cline and P.-A. Lemieux, Electroweak phase transition in two Higgs doublet models, Phys. Rev. D **55**, 3873 (1997).
[136] I. F. Ginzburg and M. Krawczyk, Symmetries of two Higgs doublet model and *CP* violation, Phys. Rev. D **72**, 115013 (2005).
[137] R. A. Battye, G. D. Brawn, and A. Pilaftsis, Vacuum topology of the two Higgs doublet model, J. High Energy Phys. 08 (2011) 020.
[138] Wolfram Programming Lab, version 13.2, Wolfram Research, Inc., (2023).
[139] A. D. Linde, Decay of the false vacuum at finite temperature, Nucl. Phys. **B216**, 421 (1983).
[140] J. R. Espinosa, T. Konstandin, J. M. No, and G. Servant, Energy budget of cosmological first-order phase transitions, J. Cosmol. Astropart. Phys. 06 (2010) 028.
[141] C. Caprini *et al.*, Science with the space-based interferometer eLISA. II: Gravitational waves from cosmological phase transitions, J. Cosmol. Astropart. Phys. 04 (2016) 001.
[142] S. J. Huber and T. Konstandin, Gravitational wave production by collisions: More bubbles, J. Cosmol. Astropart. Phys. 09 (2008) 022.
[143] M. Lewicki and V. Vaskonen, Gravitational waves from colliding vacuum bubbles in gauge theories, Eur. Phys. J. C **81**, 437 (2021).
[144] M. Kamionkowski, A. Kosowsky, and M. S. Turner, Gravitational radiation from first order phase transitions, Phys. Rev. D **49**, 2837 (1994).
[145] M. Hindmarsh, S. J. Huber, K. Rummukainen, and D. J. Weir, Gravitational waves from the sound of a first order phase transition, Phys. Rev. Lett. **112**, 041301 (2014).
[146] J. Ellis, M. Lewicki, and J. M. No, Gravitational waves from first-order cosmological phase transitions: Lifetime of the sound wave source, J. Cosmol. Astropart. Phys. 07 (2020) 050.
[147] H.-K. Guo, K. Sinha, D. Vagie, and G. White, Phase transitions in an expanding universe: Stochastic gravitational waves in standard and non-standard histories, J. Cosmol. Astropart. Phys. 01 (2021) 001.
[148] C. Caprini and R. Durrer, Gravitational waves from stochastic relativistic sources: Primordial turbulence and magnetic fields, Phys. Rev. D **74**, 063521 (2006).
[149] C. Caprini, R. Durrer, and G. Servant, The stochastic gravitational wave background from turbulence and magnetic fields generated by a first-order phase transition, J. Cosmol. Astropart. Phys. 12 (2009) 024.
[150] J. Aasi *et al.* (LIGO Scientific Collaboration), Advanced LIGO, Classical Quantum Gravity **32**, 074001 (2015).
[151] T. Hiramatsu, M. Kawasaki, and K. Saikawa, On the estimation of gravitational wave spectrum from cosmic domain walls, J. Cosmol. Astropart. Phys. 02 (2014) 031.
[152] T. J. Clarke, E. J. Copeland, and A. Moss, Constraints on primordial gravitational waves from the cosmic microwave background, J. Cosmol. Astropart. Phys. 10 (2020) 002.